SANDIA REPORT
SAND2020-10210
Printed September 2020

Sandia National Laboratories

Partitioning of Complex Fluids at Mineral Surfaces

Jeffery A. Greathouse, Daniel M. Long, Guangping Xu, Hongkyu Yoon, Iltai Kim, Katherine L. Jungjohann

Prepared by
Sandia National Laboratories
Albuquerque, New Mexico
87185 and Livermore,
California 94550

Issued by Sandia National Laboratories, operated for the United States Department of Energy by National Technology & Engineering Solutions of Sandia, LLC.

NOTICE: This report was prepared as an account of work sponsored by an agency of the United States Government. Neither the United States Government, nor any agency thereof, nor any of their employees, nor any of their contractors, subcontractors, or their employees, make any warranty, express or implied, or assume any legal liability or responsibility for the accuracy, completeness, or usefulness of any information, apparatus, product, or process disclosed, or represent that its use would not infringe privately owned rights. Reference herein to any specific commercial product, process, or service by trade name, trademark, manufacturer, or otherwise, does not necessarily constitute or imply its endorsement, recommendation, or favoring by the United States Government, any agency thereof, or any of their contractors or subcontractors. The views and opinions expressed herein do not necessarily state or reflect those of the United States Government, any agency thereof, or any of their contractors.

Printed in the United States of America. This report has been reproduced directly from the best available copy.

Available to DOE and DOE contractors from
U.S. Department of Energy
Office of Scientific and Technical Information
P.O. Box 62
Oak Ridge, TN 37831

Telephone: (865) 576-8401
Facsimile: (865) 576-5728
E-Mail: reports@osti.gov
Online ordering: http://www.osti.gov/scitech

Available to the public from
U.S. Department of Commerce
National Technical Information Service
5301 Shawnee Rd
Alexandria, VA 22312

Telephone: (800) 553-6847
Facsimile: (703) 605-6900
E-Mail: orders@ntis.gov
Online order: https://classic.ntis.gov/help/order-methods/

ABSTRACT

This report summarizes the results obtained during the LDRD project entitled "Partitioning of Complex Fluids at Mineral Interfaces." This research addressed fundamental aspects of such interfaces, which are relevant to energy-water applications in the subsurface, including fossil energy extraction and carbon sequestration. This project directly addresses the problem of selectivity of complex fluid components at mineral-fluid interfaces, where complex fluids are defined as a mixture of hydrophobic and hydrophilic components: *e.g.*, water, aqueous ions, polar/nonpolar organic compounds. Specifically, this project investigates how adsorption selectivity varies with surface properties and fluid composition. Both experimental and molecular modeling techniques were used to better understand trends in surface wettability on mineral surfaces. The experimental techniques spanned the macroscale (contact angle measurements) to the nanoscale (cryogenic electronic microscopy and vibrational spectroscopy). We focused on an anionic surfactant and a well-characterized mineral phase representative of clay phases present in oil- and gas-producing shale deposits. Collectively, the results consistently demonstrate that the presence of surfactant in the aqueous fluid significantly affects the mineral-fluid interfacial structure. Experimental and molecular modeling results reveal details of the surfactant structure at the interface, and how this structure varies with surfactant coverage and fluid composition.

ACKNOWLEDGEMENTS

We would like to thank Yifeng Wang for helpful comments. This work is supported by the Laboratory Directed Research and Development Program at Sandia National Laboratories.

CONTENTS

LIST OF FIGURES

This page left blank

ACRONYMS AND DEFINITIONS

Abbreviation	Definition
AOT	bis(2-ethylhexyl) sulfosuccinate
CMC	critical micelle concentration
Cryo-EM	cryo-electron microscopy
Cryo-FIB	cryogenic focused ion beam
Cryo-TEM	cryogenic transmission electron microscopy
DI	deionized
DTAB	dodecyltrimethylammonium bromide
FIB	focused ion beam
MD	molecular dynamics
SEM	scanning electron microscopy
TEM	transmission electron microscopy

1. INTRODUCTION

The wettability of surfaces by liquids is a direct result of intermolecular attractive and repulsive forces between the solid and liquid phases. Strong attractive forces (*e.g.*, polar liquid molecules and polar surface species) will result in surface wetting with a liquid-solid contact angle near zero. Strong repulsive forces (*e.g.*, nonpolar liquid molecules and polar surface species) will result in nonwetting behavior with a large contact angle. Surface wettability plays an important role in many energy-related applications, including energy recovery, sequestration, and water treatment. In these settings it is typically complex fluids that are in contact with surfaces. Complex fluids consist of both polar and nonpolar components, which can include water, aqueous ions, and organic species such as polymers, oils, and surfactants. Wettability is therefore a function of fluid-fluid as well as fluid-surface interactions, but the additivity of these intermolecular forces at complex interfaces is not well understood. Fundamental studies of these complex interfaces are needed to design improved complex fluids for energy-water systems. By changing fluid chemistry, the distribution and rheological properties of these fluids can be better controlled for more efficient processes.

Our long-term goal is to combine molecular-scale techniques (modeling, spectroscopy) with macroscale imagining to understand the competing roles of fluid-fluid and fluid-surface interactions on fluid partitioning at mineral surfaces. By combining molecular modeling with experimental techniques at the molecular scale (Raman spectroscopy) and the macroscale, including contact angle imaging and cryo-electron microscopy (Cryo-EM), we will provide molecular-level detail of the macroscale observations of complex fluid partitioning at mineral surfaces. In this one-year LDRD project, we focus on the adsorption of the anionic surfactant bis(2-ethylhexyl) sulfosuccinate (AOT) on a mineral surface. Mica (muscovite) was chosen as our mineral phase since it can be easily cleaved, resulting in an atomically flat surface for characterization and adsorption studies. Additionally, it is representative of clay phases present in many geologic shale formations containing oil and gas deposits.[1] Previous neutron reflectometry results indicate that AOT readily adsorbs to the mica surface in the presence of monovalent and divalent cations.[2,3]

This page left blank

2. METHODS

Details of the experimental and molecular modeling techniques will be provided in an upcoming journal article and will only be briefly summarized.

Dioctyl sulfosuccinate sodium salt (CAS Number 577-11-7, abbreviated as AOT or Na-AOT) and docusate calcium (Synonym: Bis(2-ethylhexyl) sulfosuccinate hemicalcium salt, abbreviated as Ca-AOT, CAS Number 128-49-4) were purchased from Sigma Aldrich with purity of 97% or better. All AOT studies described below are with Na-AOT unless specified otherwise. Muscovite mica (TedPella, Grade V1, 0.16 mm thick sheet) was used as the substrate for all experimental work. Freshly cleaved samples were then prepared using a knife or sticky tape.

2.1. Contact angle measurements

For contact angle measurements the mica sheet was cleaved by removing a layer of mica using sticky tape to create a freshly cleaved mica surface. Care was taken not to contaminate the freshly exposed mica surface. Preliminary testing was performed to evaluate the contact angle measurement procedure including the preparation of mica surfaces, volume of water or oil (i.e., hexadecane) droplet, wetting of mica surfaces, *etc.* The contact angle of a droplet on the mica surface was imaged using multiple systems including custom charge-coupled device cameras, confocal microscope (Zeiss LSM 900 MAT Observer Inverted Confocal system), and internal reflection system. An example setup of imaging systems and examples of contact angles and freshly cleaved mica surface are shown in Figure 2-1.

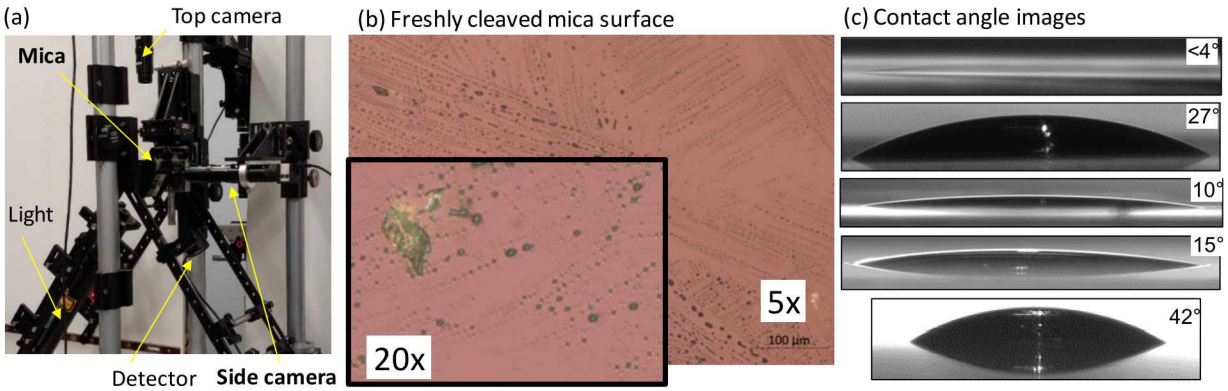

Figure 2-1. (a) A custom imaging system of internal reflection interference and sideview microscopy. (b) Differential interference contrast image of mica surface cleaved using sticky tape. Note that some surface roughness exists at the macro scale. (c) Examples of the static contact angle of a water droplet (10 µl volume) on freshly cleaved mica surface and original commercial surface (top two images) and static contact angle images of hexadecane on the surface of freshly cleaved mica, glass, and plastic surfaces (bottom three images).

Based on the preliminary testing a 2 µl volume of droplet was chosen to minimize the variation of contact angle partly due to surface roughness o by the peeling method at the macro scale. A small volume of the droplet also made it easier to perform multiple contact angle measurements on the same freshly cleaved mica surface. For the oil phase, hexadecane was used. For the contact angle of hexadecane on the mica surface in the presence of water, the cleaved mica surface was soaked in water with different Na-AOT concentrations from near the critical micelle concentration (CMC)

(0.0973 % by weight) to pure water with two intermediate concentrations (0.0124 % and 0.00058 %). To prepare the water-wetted mica surface, freshly cleaved mica was soaked in the aqueous solution for 1-4 days with and without stirring. It was observed that ~ 3 days of pre-equilibrium period was enough to produce reproducible results, meaning that cation exchange on the mica surface would be complete with this time period. With the mica taken out of the solution, any visible thick water film on the mica surface was gently removed with nitrogen or helium gas flow.

2.2. Cryo-electron microscopy

Investigating the mica/Na-AOT solution interface requires a careful approach; steps include: sample mounting, vitrification, Pt coating, mechanical sample transfer, Pt cap coating, the cryogenic focused ion beam (cryo-FIB) process, and the cryogenic transmission electron microscope (cryo-TEM) loading and imaging process. The use of cryo-FIB liftout for making the TEM sample required the use of a dual-purpose FIB grid and scanning electron microscope (SEM) stub holder. We developed a sample mounting technique based around a standard SEM pin stub where the mica was adhered to the SEM pin stub via carbon or copper tape, which was wrapped around the edges of the stub, and then mechanically exfoliated to a few microns thickness (using the Scotch tape method). This process kept the mica rigid and adhered to the adhesive while being rapidly frozen to cryogenic temperatures. Exfoliation continued until fringes were visible under an optical microscope. Next, 2 μL of the Na-AOT deionized (DI) water solution was immediately pipetted onto the center of the mica sheet mounted on the SEM pin.

Accurate examination of the mica/Na-AOT solution interface required that the water be vitrified, or amorphously frozen. Slush N_2, produced by vacuum pumping on liquid nitrogen until solid nitrogen began to form, was used to vitrify the solution because it was easy to reproduce and kept the sample clean. Once the sample was plunged into the slush N_2, it was immediately transferred into a Leica cryo-suite of systems, including a cryo-load station, cryo-transfer shuttle, cryo-sputtercoater, and the cryogenic stage with a liftout needle inside a Thermo Fisher Scientific Scios 2 FIB/SEM. The sample was kept below −150 °C throughout the entire cryogenic process to avoid devitrification.

Once inside the FIB, the electron beam energy was kept at 5 kV and beam current at 50 pA or less, and the Ga ion beam energy was kept at 16 kV and the beam current was kept below a few nanoamps in order to reduce damage and minimize heating. First, the region of interest from which to create a FIB sample from was located. The edge of the vitrified droplet, shown in Figure 2-2, was chosen as the region of interest for all liftouts because of its ideal ice thickness which made the FIB process the easiest there.

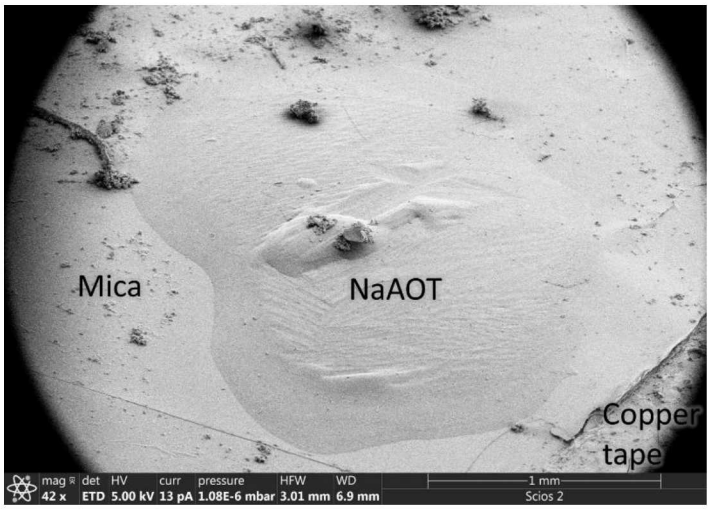

Figure 2-2. Low magnification SEM image of Na-AOT solution on mica. The image is tilted with respect to the electron beam in order to enhance the visibility of the topography.

Once a region of interest was confirmed, organometallic Pt was condensed and cured onto the surface of the sample to protect the region of interest from damage and heating. Trenches were then milled at a few nanoamps and in a similar fashion to the room temperature liftout process. Mechanical attachment to the liftout needle required a series of organometallic Pt condensation and fine ion-beam milling steps in order to ensure a robust connection.

Attachment of the thinned lamella to the grid required several steps for attaching to the needle and several additional milling patterns (Figure 2-3). Once the initial mechanical connection was made to the grid, large cuts were made around the perimeter of the sample to cause redeposition into the connection, which added mechanical stability.

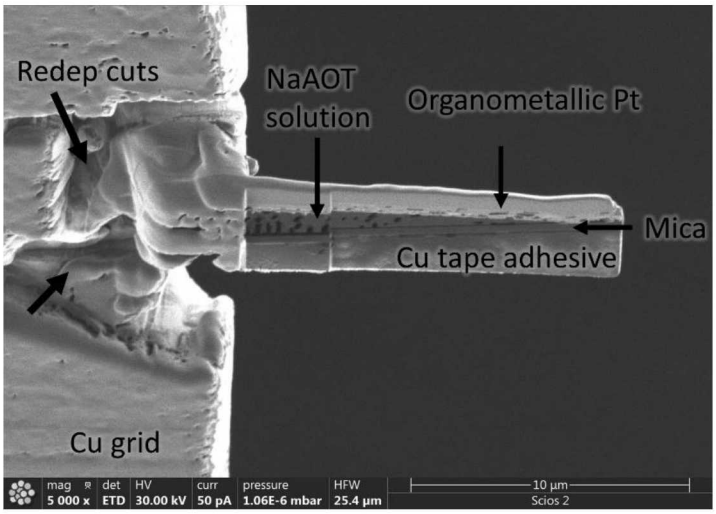

Figure 2-3. Attachment to the grid with excessive reposition patterns around the sample.

Thinning the sample to electron transparency was similar to a room temperature FIB polishing process. Very low beam currents, tens to a hundred picoamps, and small tilts of ± 1-2° were used to thin to ~ 100 nm thickness, followed by a final polish at 5 kV 48 pA at ± 5° to remove most of the surface FIB damage. Once thinned, the sample was stored in an LN2 storage dewar until the sample could be imaged in the TEM.

2.3. Adsorption and spectroscopic measurements

Transmission infrared spectra were collected using a Thermo Fisher iN10 microscope for muscovite and Na-AOT. Raman spectra were obtained using Horiba XploRa plus microscope. All Raman measurements were conducted using exactly the same configuration: 50x objective, 532 nm laser with 600 gratings. About 2 μL aqueous AOT solutions were dropped on a freshly peeled muscovite surface which is tilted slightly. The Raman and infrared spectra were obtained after the AOT was air dried.

The CMC for Na-AOT and Ca-AOT is 2.5 mM and 0.5 mM, respectively.[2] The AOT solutions used in the spectroscopy measurements (2.29 mM for Na-AOT and 0.49 mM for Ca-AOT, respectively) were slightly below the CMC.

Different pieces of muscovite samples were soaked into DI water, Ca-AOT, Na-AOT and NaCl (2.26 mM) and left on a shaker to examine the ion exchange for a few days. The muscovite pieces were then air dried before the infrared spectra measurements.

2.4. Molecular modeling

Model systems for molecular dynamics (MD) simulations consisted of a mica surface in contact with an aqueous phase consisting of AOT anions and cations to balance both the surface charge and the AOT charge. Aqueous cations ranged from weakly hydrating monovalent alkali earth (Na^+, K^+, Cs^+) and strongly hydrating divalent alkaline earth (Mg^{2+}, Ca^{2+}). The model mica surface consisted of 32 negative charge sites, which provides an upper limit of 32 AOT anions for monolayer coverage. Therefore, separate simulations were performed for 32, 48 and 64 AOT anions to include the possibility of AOT bilayer formation seen in previous studies.[2,3] For each model system, simulations were run for at least 100 ns to confirm that the equilibrium AOT structure had been achieved. All MD simulations were performed using the LAMMPS code[4] at a thermostat temperature of 300 K. Two-dimensional periodic boundary conditions were used so that the aqueous phase was in contact with only one mica surface. Example initial and final configurations are shown in Figure 2-4.

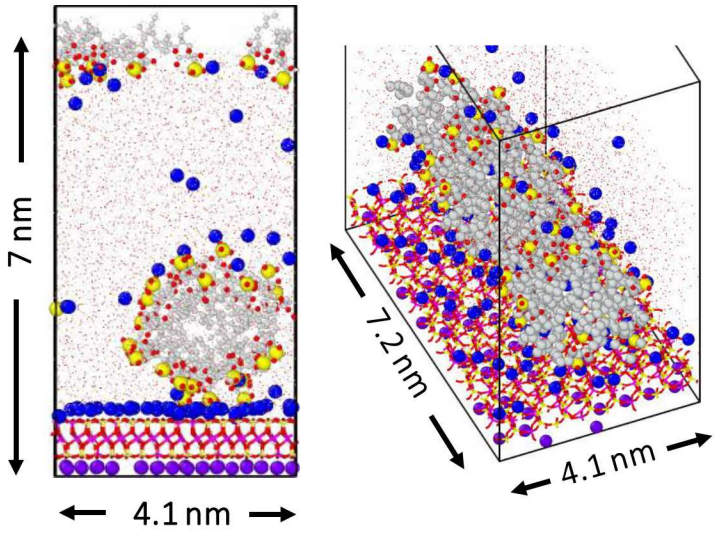

Figure 2-4. MD simulation snapshot showing the equilibrium configuration of 32 AOT anions with Na^+ cations (left). The alternate view (right) shows the cylindrical micelle structure. The mica layer is shown as sticks. Charge balancing cations K^+ (purple, bottom) and Na^+ (blue) are shown as large spheres. Atoms in the AOT anions are shown as follows: C (gray), O (red), S (yellow). Water oxygen atoms are shown as red dots. Hydrogen atoms are omitted for ease of viewing.

This page left blank

3. RESULTS

3.1. Contact angle measurements

Contact angles of a hexadecane droplet on the mica surface under six different conditions are shown in Figure 3-1. Contact angles of hexadecane on dry mica surfaces (fresh cleaved, stored in desiccator and ambient air in Figure 3-1(a-c) show relatively consistent results over a range of ~9° to ~10°, while results on the wet surface show higher contact angles and more variability, depending on preparation conditions. These results clearly show that the contact angle of hexadecane increases in the presence of water film on the mica surface and may increase with increasing the thickness of water film in Figure 3-1(e-f) compared to in Figure 3-1d. It is not conclusive without the measurement of water film thickness, but the experimental results may indicate that drying in ambient air and room temperature (20-25 °C) may decrease the thickness of the water film, creating a transition state between monolayer water film and thick water films with bulk water properties. Hexadecane is known to have no long-range order at the liquid-water interface, and freshly cleaved mica has been wetted in water for at least one day to ensure the desorption of potassium cations from the cleaved surface would reach the equilibrium state. Hence, the change of contact angle in different wet conditions may be attributed to the different water properties of the water films. For the following contact angle measurements, the mica surface was prepared by slowly blowing nitrogen or helium gas over the wet mica after being removed from aqueous solution. In this way, the repeatability of the contact angle results was relatively consistent within ±1.5°.

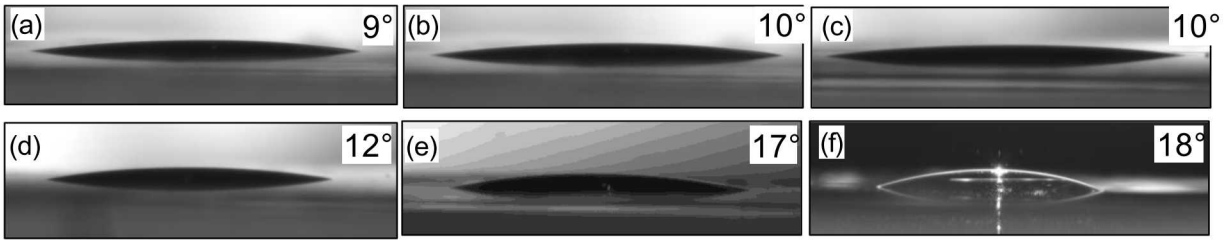

Figure 3-1. Contact angles of hexadecane on (a-c) dry mica surfaces (a: fresh cleaved, stored for two days in (b) desiccator and (c) ambient air), and (d-f) wet mica surface with (d) drying in ambient air for two days after wetting in water for at least one day, (e) nitrogen gas drying after wetting in water for one day, and (f) nitrogen gas drying after wetting in water for four days. All mica surfaces were cleaved using sticky tape.

The effect of AOT on the contact angle of hexadecane has been evaluated by conditioning the freshly cleaved mica surface with nanopure water and different AOT concentrations as shown in Figure 3-2. The contact angle of hexadecane clearly increases with increasing AOT concentration in AOT solution, indicating that the arrangement of AOT molecules in the water film increases the aqueous film hydrophobicity. The spreading behavior of hydrocarbons on a water surface in the presence of a gas phase is characterized as three distinctive types from partial wetting, pseudo-partial wetting, and complete spreading.[5,6] Figure 3-2 shows that the spreading of hydrocarbon changes from pseudo-partial spreading to partial wetting types as shown in the contact angle values. Given a high surface energy of the cleaved mica surface (~ 500 mJ/m^2) and the water film thickness being thicker than the monolayer water film, the change of spreading or contact angle of hexadecane can be attributed to the AOT interaction in the water film and at the mica surface. The increasing

trending of contact angle (i.e., less spreading) with increasing anionic AOT concentration in the bulk phase of wetting solution indicates that the arrangement of AOT anions at the interfacial film of liquid-vapor interface provides the hydrophobic interaction at the liquid-vapor interface. This indicates that the tail part of AOT may be more accumulated at the liquid-vapor interface, resulting in a higher contact angle at higher AOT concentration. Interestingly, Matsubara et al.[7] showed that the spreading coefficient of hydrocarbons on aqueous films increased with increasing cationic surfactant (dodecyltrimethylammonium bromide, DTAB) concentration in aqueous solution. Comparison of this work with anionic AOT and cationic DTAB clearly indicates that the surfactant behaves differently depending on surfactant charge and how surfactants interact with the solid phase and at the liquid-vapor interface.

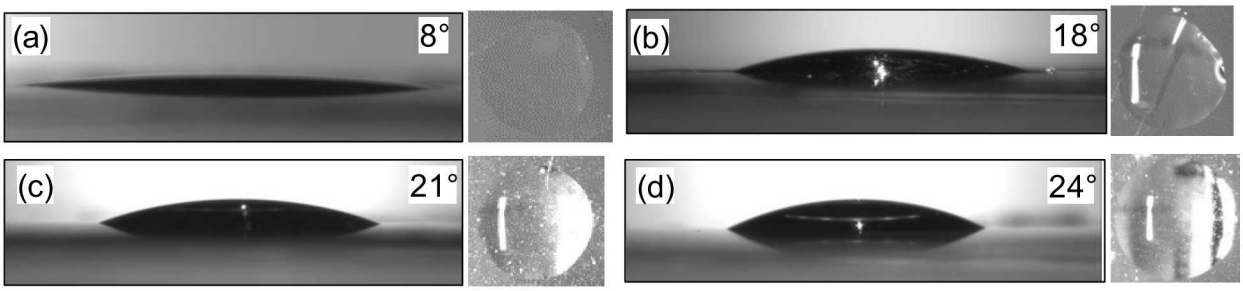

Figure 3-2. Contact angle of a hexadecane droplet on a cleaved mica surface conditioned with Na-AOT solutions: (a) pure water, (b) AOT 0.00058% by weight, (c) AOT 0.0124% by weight, and (b) AOT 0.0973% by weight.

3.2. Cryo-electron microscopy

TEM imaging was performed with a Thermo Fisher Scientific Talos 120C TEM operated at 120 kV with the sample kept near liquid nitrogen temperatures in a Gatan 626 cryo-TEM holder. This microscope was used because it has a lower operating voltage which allowed for higher contrast of lighter materials, such as organics, and because it had an enlarged cryogenic contamination shield which kept the sample ice-free and maintained a high vacuum environment around the specimen. Figure 3-3 and Figure 3-4 are the low and high magnification TEM images of a sample with a vitreous 2.3 mM NaAOT solution against the mica surface. The low magnification image in Figure 3-3a displays the extensive ice contamination, highlighting the difficulty of these experiments. (Extensive efforts to find the source of the ice contamination eventually concluded that the manufacturer-supplied tubing was not suitable for high purity gas delivery. Exchanging the thermoplastic polyurethane tubing for a stainless-steel tubing reduced the ice contamination almost entirely). The high magnification image in Figure 3-3b shows the nanoscale structure of the interface. The visible mica basal planes indicate that the interface was normal to the incident beam which enabled a precise view of the interface. A ~5 nm thick layer of disordered particles, each ~2-3 nm in diameter, resided at the mica surface and many of the particles had a thin (1-2 nm) water layer between them and the mica surface. All of these features and their absolute sizes agree well with the mica/Na-AOT solution interface structure predicted by MD. To ensure that the 2-3 nm particles were in fact micelles, we conducted a control study using pure deionized water, shown in Figure 3-4. Mica in deionized water showed no evidence of 2-3 nm particles at the mica interface, which proved that the spherical particles were in fact micelles and that they were only present in the Na-AOT solution. These results display the effectiveness of MD to simulate these complex molecule interfaces on mineral surfaces and demonstrate that the combination of cryo-EM and MD are an effective combination for studying mineral/liquid interfaces.

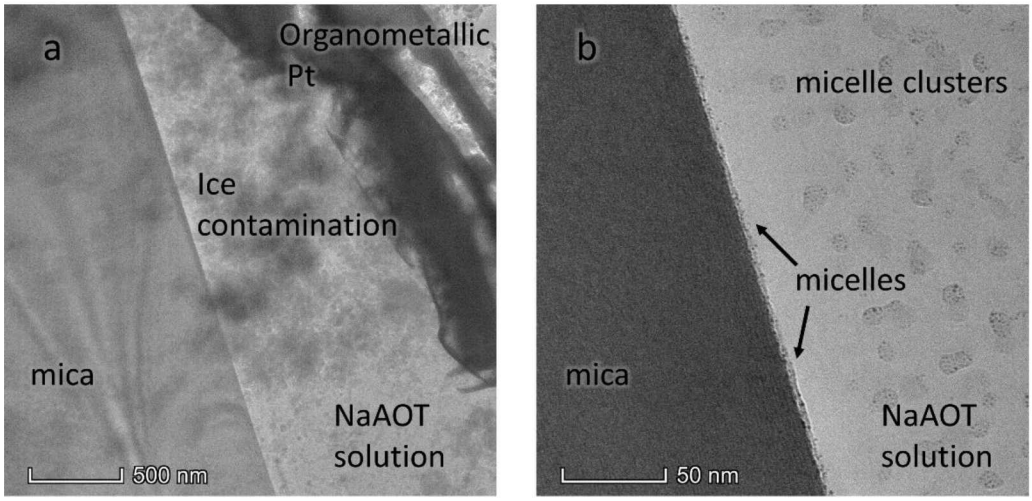

Figure 3-3. (a) Low and (high) magnification images of the mica/NaAOT solution interface.

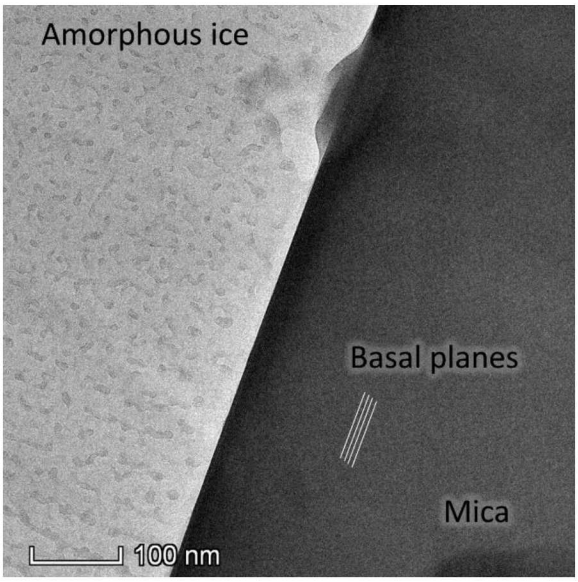

Figure 3-4. Image of control sample showing absence of particles at the mica surface.

We must note that in both Figure 3-3 and Figure 3-4, we see larger (5-10 nm) shapes in the bulk of the amorphous ice. Figure 3-5 shows a region of the mica/Na-AOT solution interface liftout sample that was not fully thinned and polished. Extensive texture in this region indicates that the surface damage was extensive here and that the final polishing still needs to be tuned. The features observed in Figure 3-3 and Figure 3-4 are therefore due to surface damage which is easy to create but difficult to avoid due to ice's high milling rate under the ion beam.

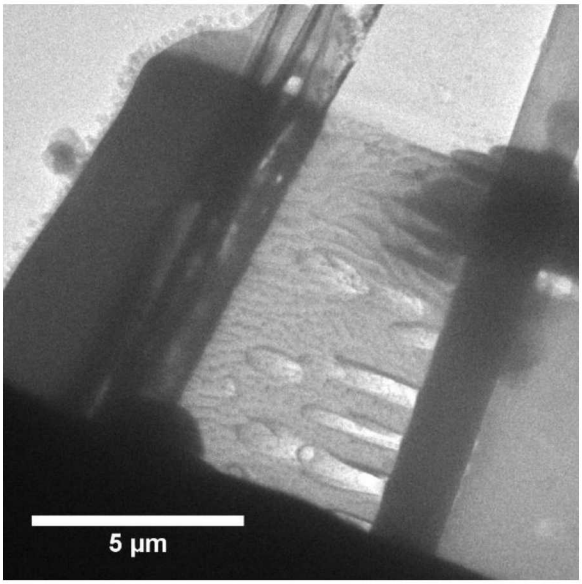

Figure 3-5. Na-AOT solution that was polished with 100 pA beam shows extensive surface roughness from high beam current exposure. No final polishing was performed on this sample.

3.3. Adsorption and spectroscopic measurements

Ammonium is produced during the diagenesis of organic matter in sediments. Ammonium can easily substitute potassium in K-bearing minerals such as muscovite. Therefore, it is normal to have infrared peaks that are indicative of ammonium in muscovite, especially at 2800-3400 cm^{-1} and ~1428 cm^{-1}, caused by N-H stretching and bending (Figure 3-6 and Figure 3-7).[8] Within a little more than two days, the NH_4^+ in the muscovite sample was cation exchanged by Na^+ (or Ca^{2+} in Ca-AOT) in the AOT solution as well as in the NaCl solution (Figure 3-7). As expected, muscovite soaked in DI water has the same infrared spectrum as the original sample (Figure 3-7).

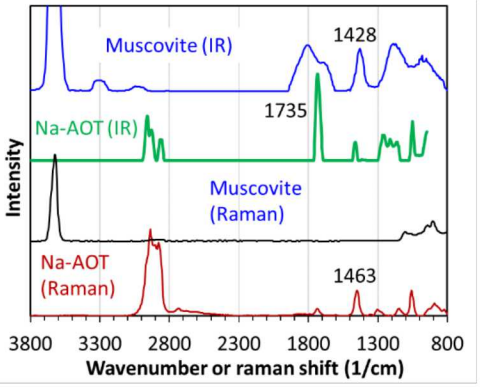

wavenumber (cm^{-1})	mode
3630	OH vibration (mica)
2800 – 3050	CH_2, CH_3 stretching vibration (AOT tail)
1735	C=O stretching vibration (AOT head)
1463	CH_2, CH_3 bending vibration (AOT tail)
1057	S=O stretching vibration (AOT head)

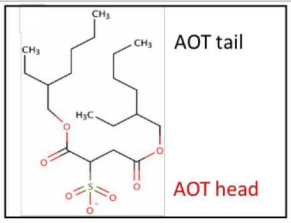

Figure 3-6. (a) Transmission infrared and Raman spectra for muscovite and Na-AOT; (b) list of major vibration peaks; (c) structure of AOT illustrating the head (in red) and tails.

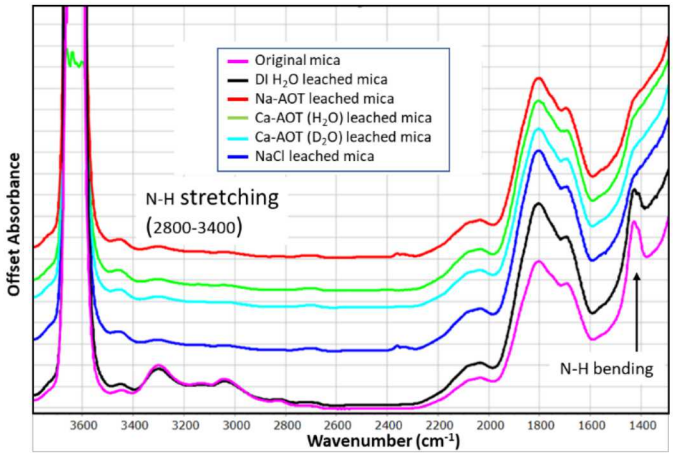

Figure 3-7. Transmission infrared spectra for original muscovite and the ones soaked in solutions showing the disappearing of peaks at 2800-3400 cm^{-1} and ~1430 cm^{-1} except for DI water leached muscovite, confirming the cation exchange between NH_4^+ and Na^+ in the AOT (or NaCl) solutions.

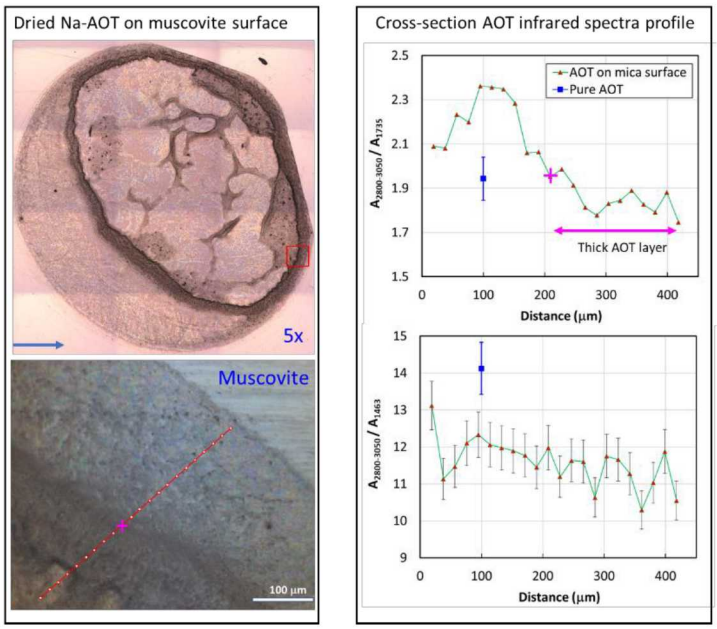

Figure 3-8. Cross-section transmission infrared spectra for dried Na-AOT on the muscovite surface. Left panel – optical image showing a drop of AOT solution on the tilted muscovite surface (represented by the arrow), and cross-section line with pink "+" marking the approximate boundary of thick and thin AOT layers in the area showing as pink square box in the upper left panel. Right panel – the area ratios of peaks at 2800-3050 cm^{-1} and 1735 cm^{-1}, i.e., tail/head ratio, and peaks at 2800-3050 cm^{-1} and 1463 cm^{-1}, i.e., tail/tail ratio. The error bars show ± 5%. The pure muscovite spectrum was subtracted from the measured infrared spectra. The pure Na-AOT spectrum is the average of 6 different measurements with a generic error bar of ± 5%.

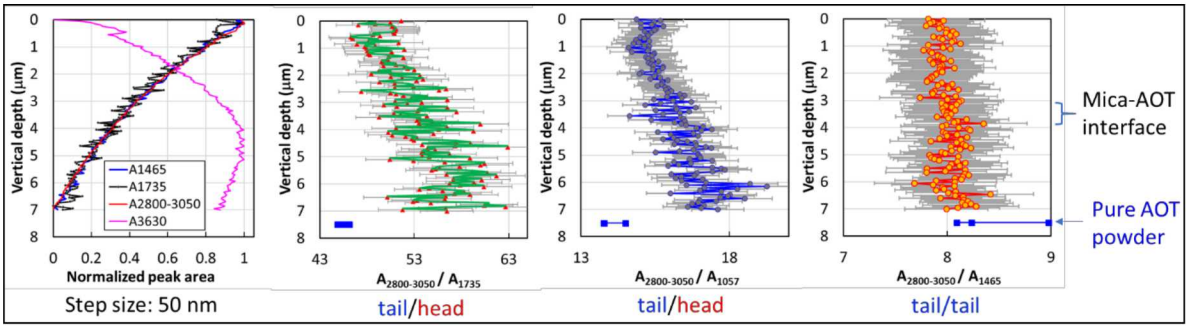

Figure 3-9. Depth profile of Raman spectra across the interface of muscovite and AOT. As shown in Figure 3-8, the thickness of the Na-AOT layer is estimated to be ~ 3-4 microns. The ratios of tail/head areas (i.e., $A_{2800\text{-}3050}/A_{1735}$ and $A_{2800\text{-}3050}/A_{1057}$) are slightly higher than the bulk Na-AOT ratio near the muscovite/Na-AOT interface whereas the ratio of tail/tail areas (i.e., $A_{2800\text{-}3050}/A_{1435}$) is nearly constant. The error bars show ± 5%.

As shown in Figure 3-6, the integrated areas for infrared and Raman peaks attributed to the functional groups on the AOT head and tail are calculated, 2800-3050 cm^{-1} (tail), 1735 cm^{-1} (head), 1465 cm^{-1} (tail), 1057 cm^{-1} (head). Whereas the absolute value of the peak depends on the differences in samples and experimental settings, the ratios of the peaks are relatively stable and reproducible

with similar experimental conditions. Pure AOT has $A_{2800\text{-}3050}$ / A_{1735} of 1.94 ± 0.015 (n = 6, 2σ) and $A_{2800\text{-}3050}$ / A_{1465} of 14.13 ± 0.015 (n = 6, 2σ).

The measured $A_{2800\text{-}3050}$ / A_{1735} infrared spectra ratios for dried AOT on the muscovite surface range from 1.8 to 2.4 (Figure 3-8). These ratios change with the thickness of the AOT layer. At cross sections with a thick-AOT-layer, the ratios are slightly lower than pure AOT, but the ratios are clearly higher than AOT at thinner-AOT-layers (Figure 3-8). The thick-AOT-layer is estimated to be ~ 3-4 μm thick (Figure 3-9) and the thinner layer is estimated to be 1 μm or less. In contrast, there are less variations in $A_{2800\text{-}3050}$ / A_{1465} ratios, 10.5 to 12.2 except one at 13, in the cross section (Figure 3-8). These ratios are less than the pure AOT ratio, possibly due to the interference of the peak at 1465 cm^{-1} by the N-H bending mode at 1428 cm^{-1} which is only seen in the transmission infrared spectrum (Figure 3-7). The different tail/head but relatively constant tail/tail ratios suggests that there is head-tail re-orientation for AOT near the muscovite interface, and this feature is not noticeable in bulk measurement unless with very thin AOT layers.

The AOT-muscovite interface can be located with confocal Raman microscopy with the relative intensity of the peak at 3630 cm^{-1}, attributed to layer hydroxyl groups in muscovite, and different AOT peaks (Figure 3-9). The intensity of the 3630 cm^{-1} peak increases to a maximum at a depth of 4 μm with a continuous decrease of AOT peaks (Figure 3-9), and thus the interface is inferred at depth of 3 – 4 μm. At a depth of 0 μm, the tail/head ratios ($A_{2800\text{-}3050}$ / A_{1735} and $A_{2800\text{-}3050}$ / A_{1465}) are close to the ratios in pure AOT powder, and the tail/head ratios increase slightly with the increase of depth to the interface whereas the tail/tail ratios are nearly constant, within the range of pure AOT powder (Figure 3-9). As consistent with the infrared spectra, there is an increase in tail/head ratio approaching the interface, suggesting re-alignment of AOT molecules at the AOT-muscovite interface with higher density of tails compared to heads.

Note that the depth interval is 50 nm and the horizontal analyzed area is up to 1 μm, and these are much larger than the normal micelle diameters (in the order of a few nanometers) or micelle-rich layers near the interface as observed from Cryo-EM (Figure 3-3). Therefore, the measured spectra variations near the interface is a result of the nugget effect of micelle-rich layers.

3.4. Molecular modeling

MD results indicate that the surfactant structure was determined by the number of AOT anions present in the model system. Cylindrical micelles formed at lower AOT concentration (32 AOT, Figure 2-4) since there were not enough AOT anions to form a bilayer. AOT bilayers formed when sufficient number of AOT anions were present (48 or 64 AOT, Figure 3-10).

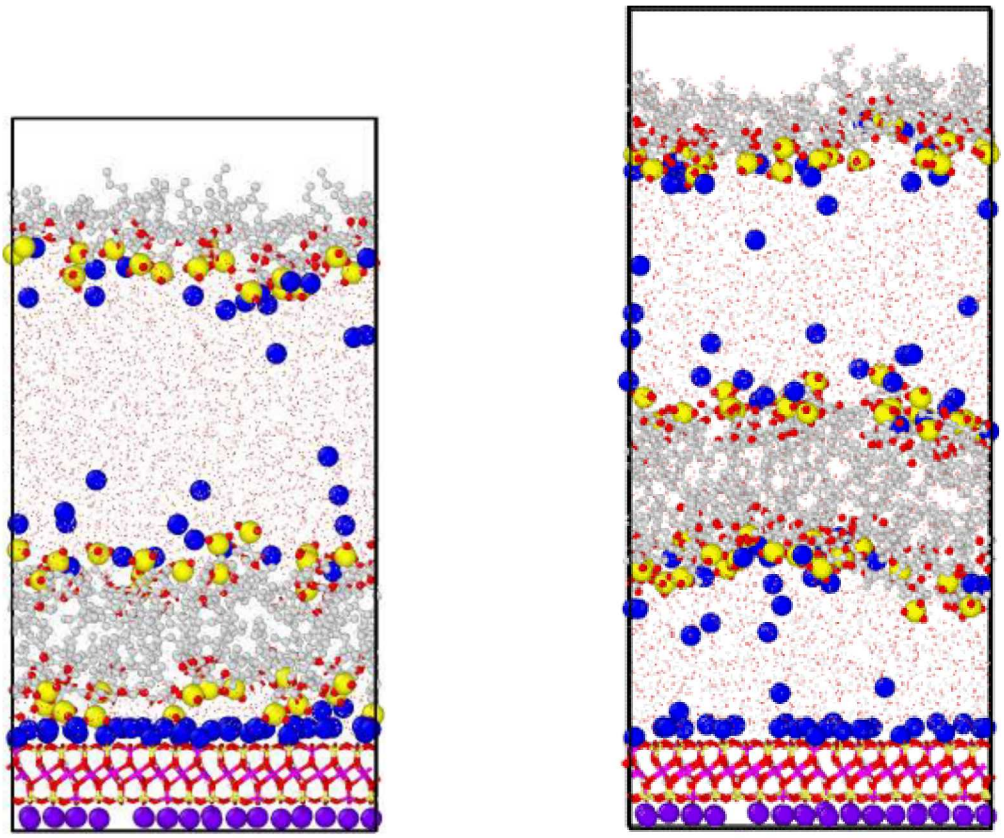

Figure 3-10. MD simulation snapshots showing the equilibrium configurations for 48 AOT anions (left) and 64 AOT anions (right) with Na^+ cations. See Figure 2-4 for atom colors and rendering.

The surfactant structures can be quantified by examining one-dimensional atomic density profiles. Results from simulations with Na^+ cations are shown in Figure 3-11 and are representative of the other cations simulated. The adsorbed micelle structure seen in the 32 AOT systems is characterized by the broad sulfur peak between 12 - 40 Å. Bilayers in the 48 AOT and 64 AOT systems are characterized by two sulfur peaks on either side of a thin hydrophobic region of zero sulfur density. The hydrophobic region consists primarily of AOT carbon atoms corresponding to the aliphatic tails of the surfactants (Figure 3-11). Note that water molecules and Na^+ cations are also excluded from the bilayer region. The density profiles also indicate that the location of the AOT bilayer depends on AOT content. With only 48 AOT present, the bilayer is adsorbed on the mica surface with only a thin layer of hydrated cations between sulfate head groups and the surface. With an excess of AOT present (64 AOT), bilayers were separated from the mica surface by water layers approximately 10 – 20 Å thick. Of the 64 AOT systems, only the K^+ cation resulted in an adsorbed bilayer with an interfacial structure similar to the 48 AOT systems. Finally, the AOT sulfur profiles were used to estimate the thickness of AOT micelles and bilayers: 2.2 – 3.0 nm for micelles and 2.0 – 2.4 nm for bilayers. The bilayer thicknesses are in good agreement with those measured experimentally at the mica surface (2.2 nm),[2] which provides a good validation of the MD methods.

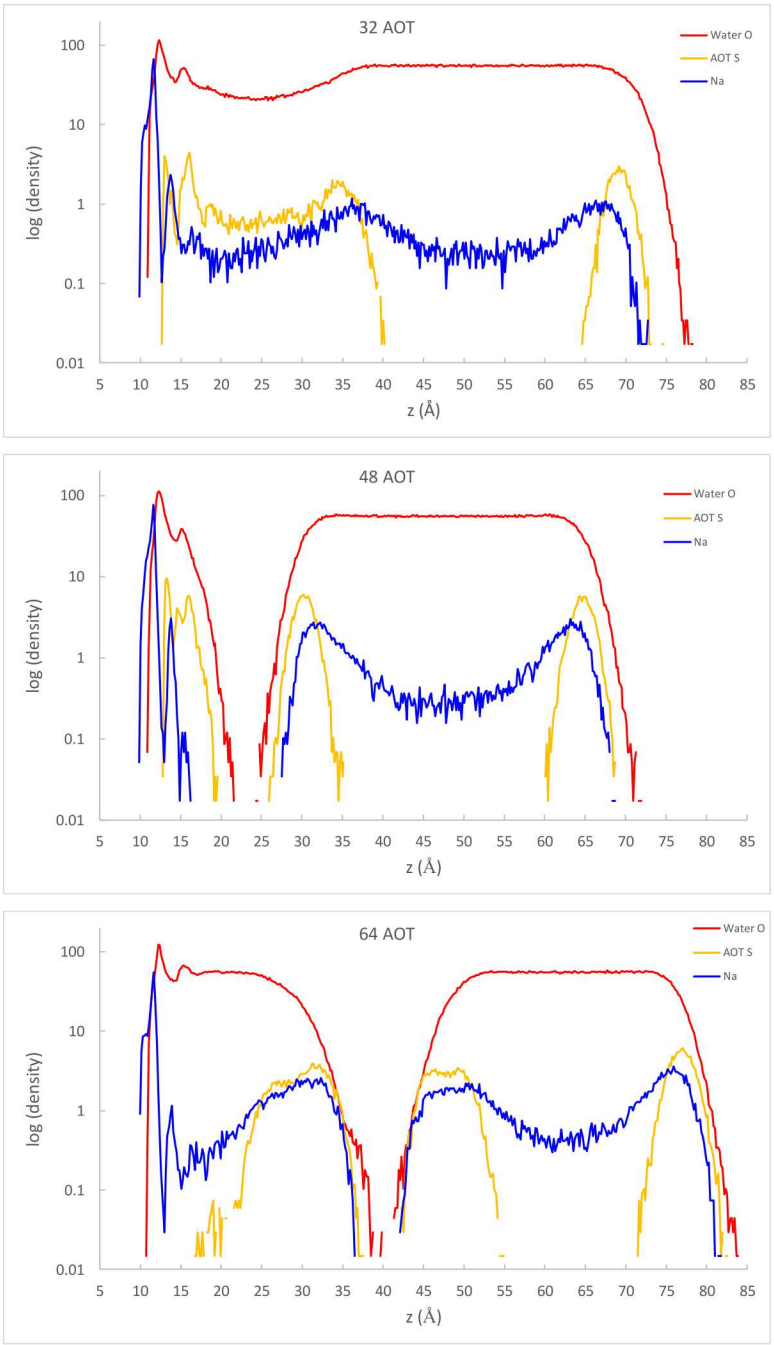

Figure 3-11. Atomic density profiles showing the surfactant structure from MD simulations of 32 AOT (top), 48 AOT (middle), and 64 AOT (bottom) with Na^+ cations. Profiles show densities of water O atoms (red), AOT S atoms (yellow), and Na^+ cations (blue) as a function of height above the mica surface. Profiles were averaged over the final 20 ns of the simulations.

Although the type of cation present in the aqueous phase does not significantly influence the AOT micelle or bilayer structures, the cation does control the binding mechanism between AOT sulfate groups and surface cations. As seen in Figure 3-12, weakly hydrating cations such as K^+ are able to

coordinate directly to sulfate oxygen atoms, typically in monodentate fashion (K-$O_{sulfate}$ coordination number of 1). Examples of AOT sulfate groups binding directly to surface Na^+ cations can be seen in the MD snapshots from Figure 2-4 and Figure 3-10. Strongly hydrating cations such as Ca^{2+} remain fully hydrated and do not coordinate directly to sulfate oxygen atoms. In this case, cation binding to AOT occurs through hydrogen bonding between coordinating water molecules and sulfate oxygen atoms. Regardless of cation-AOT binding, these strong interactions serve to bind AOT anions to a negatively charged mineral surface.

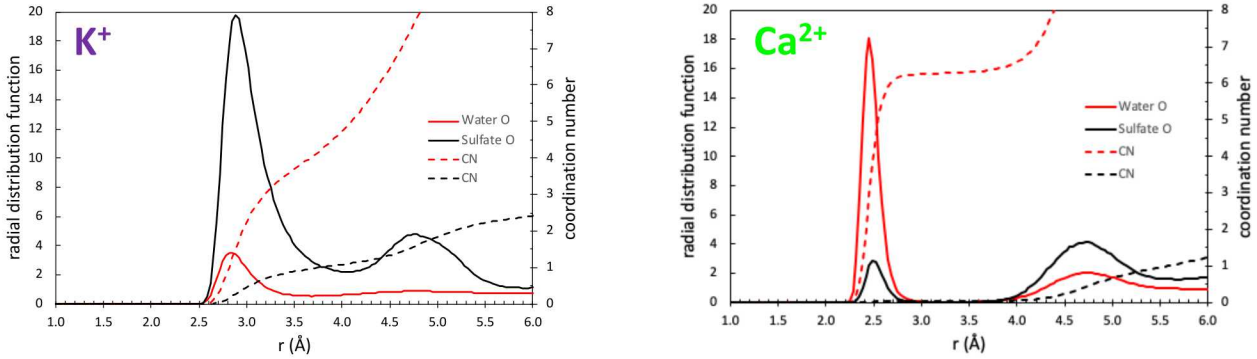

Figure 3-12. Average radial distribution function plots from MD simulations, showing S-O distances and running coordination number (CN) for 32 AOT systems with K^+ and Ca^{2+} cations. Correspond to the final 20 ns of the simulations.

The effect of increased temperature on AOT interfacial structure was also investigated. The final configuration of each 32 AOT system was heated to 350 K over a 20-ns simulation and then simulated at 350 K for an additional 20 ns. This higher temperature is consistent with many shale reservoirs, allowing us to investigate AOT-mica interactions at both laboratory and field temperatures. Heating to 350 K did not change the adsorption properties of AOT—the micelles remained adsorbed to the surface through cation bridging. However, heating did result in a subtle transition from micelle to bilayer structure for all cations. Additionally, heating did enable more sulfate head groups to bind directly to surface cations, but this process does not appear to be linked to bilayer formation.

4. CONCLUSION

Experimental and molecular modeling techniques were used to better understand trends in wettability on mineral surfaces due to interactions with complex fluids. The experimental techniques spanned the macroscale (contact angle measurements) to the nanoscale (cryogenic electronic microscopy and vibrational spectroscopy). We focused on the adsorption of an anionic surfactant (AOT) on a well-characterized mineral phase (mica). Collectively, the results consistently demonstrated that the presence of AOT in the aqueous fluid significantly affects the fluid structure at the mica surface. Both contact angle measurements and vibrational spectroscopy revealed changes in fluid-surface and fluid-fluid properties when AOT was present. Additionally, the wetting properties of a nonpolar fluid (hexadecane) on a water-coated mica surface change as the AOT concentration in the aqueous phase is varied. Cryo-EM provided a snapshot of the mica-AOT interface, revealing the presence of adsorbed AOT micelles at low concentration. The presence of adsorbed micelles was confirmed by molecular dynamics simulations. The simulations also showed that AOT bilayers form at higher concentration, consistent with published neutron reflectivity results.

Although AOT is an anionic surfactant, binding to the negatively charged mica surface occurs through a cation bridging mechanism. The simulations further revealed that weakly hydrating monovalent cations bind AOT by direct interaction with polar (sulfate) head groups, while strongly hydrating divalent cations maintain a full hydration shell and interact with AOT only through hydrogen bonding.

This project provides the foundation for additional multidisciplinary studies of complex fluid behavior at mineral surfaces and in mineral nanopores. Understanding the properties of such fluids in subsurface environments will enable breakthroughs in designing complex fluids for energy-water systems.

REFERENCES

1. A. G. Ilgen, J. E. Heath, I. Y. Akkutlu, L. T. Bryndzia, D. R. Cole, Y. K. Kharaka, T. J. Kneafsey, K. L. Milliken, L. J. Pyrak-Nolte, and R. Suarez-Rivera. "Shales at all scales: Exploring coupled processes in mudrocks." *Earth-Sci. Rev.*, *166*, (2017): pp. 132-152.
2. F. J. Allen, L. R. Griffin, R. M. Alloway, P. Gutfreund, S. Y. Lee, C. L. Truscott, R. J. L. Welbourn, M. H. Wood, and S. M. Clarke. "An Anionic Surfactant on an Anionic Substrate: Monovalent Cation Binding." *Langmuir*, *33*, (2017): pp. 7881-7888.
3. F. J. Allen, C. L. Truscott, P. Gutfreund, R. J. L. Welbourn, and S. M. Clarke. "Potassium, Calcium, and Magnesium Bridging of AOT to Mica at Constant Ionic Strength." *Langmuir*, *35*, (2019): pp. 5753-5761.
4. S. J. Plimpton. "Fast Parallel Algorithms for Short-Range Molecular Dynamics." *J. Comp. Phys.*, *117*, (1995): pp. 1-19.
5. H. Matsubara, A. Aratono, K. M. Wilkinson, and C. D. Bain. "Lattice model for the wetting transition of alkanes on aqueous surfactant solutions." *Langmuir*, *22*, (2006): pp. 982-988.
6. S. R. Nellis, H. Yoon, C. J. Werth, M. Oostrom, and A. J. Valocchi. "Surface and Interfacial Properties of Nonaqueous-Phase Liquid Mixtures Released to the Subsurface at the Hanford Site." *Vadose Zone J.*, *8*, (2009): pp. 343-351.
7. H. Matsubara, N. Ikeda, T. Takiue, M. Aratono, and C. D. Bain. "Interfacial films and wetting behavior of hexadecane on aqueous solutions of dodecyltrimethylammonium bromide." *Langmuir*, *19*, (2003): pp. 2249-2253.
8. S. R. Boyd. "Determination of the ammonium content of potassic rocks and minerals by capacitance manometry: A prelude to the calibration of FTIR microscopes." *Chem. Geol.*, *137*, (1997): pp. 57-66.

DISTRIBUTION

Email—Internal

Name	Org.	Sandia Email Address
Nancy Brodsky	08865	nsbrods@sandia.gov
Benjamin Cook	08860	bkcook@sandia.gov
Hongyou Fan	08865	hfan@sandia.gov
Jeffery Greathouse	08865	jagreat@sandia.gov
Katherine Junghohann	01881	kljung@sandia.gov
Moo Lee	08864	mylee@sandia.gov
Daniel Long	01881	dmlong@sandia.gov
Jeffrey Nelson	01880	jsnelso@sandia.gov
Erik Webb	06160	ekwebb@sandia.gov
Ryan Wixom	01881	rrwixom@sandia.gov
Guangping Xu	08865	gxu@sandia.gov
Hongkyu Yoon	08864	hyoon@sandia.gov
Technical Library	01977	sanddocs@sandia.gov

Email—External

Name	Company Email Address	Company Name
Isaac Kim	Iltai.Kim@tamucc.edu	Texas A&M University, Corpus Christi

Hardcopy—Internal

Number of Copies	Name	Org.	Mailstop
5	Jeffery Greathouse	08865	0754

This page left blank

Sandia National Laboratories

Sandia National Laboratories is a multimission laboratory managed and operated by National Technology & Engineering Solutions of Sandia LLC, a wholly owned subsidiary of Honeywell International Inc. for the U.S. Department of Energy's National Nuclear Security Administration under contract DE-NA0003525.